(2) P. E. Riley and K. Seff, *J. Phys. Chem.*, **79**, 1594 (1975).
(3) K. Seff, *Acc. Chem. Res.*, **9**, 121 (1976).
(4) The structural frameworks of the various aluminosilicate zeolites are described in detail in D. W. Breck, "Zeolite Molecular Sieves", Wiley, New York, 1974.
(5) R. Y. Yanagida, T. B. Vance, Jr., and K. Seff, *Inorg. Chem.*, **13**, 723 (1974).
(6) K. Klier and M. Rálek, *J. Phys. Chem. Solids*, **29**, 951 (1968).
(7) K. Klier, *Adv. Chem. Ser.*, **No. 101**, 480 (1971).
(8) J. Texter, D. H. Strome, R. G. Herman, and K. Klier, *J. Phys. Chem.*, **81**, 333 (1977).
(9) W. deWilde, R. A. Schoonheydt, and J. B. Uytterhoeven, *ACS Symp. Ser.*, **No. 40**, 132 (1977).
(10) R. G. Herman and D. R. Flentge, *J. Phys. Chem.*, **82**, 720 (1978).
(11) C. Naccache and Y. Ben Taarit, *Chem. Phys. Lett.*, **11**, 11 (1971).
(12) E. F. Vansant and J. H. Lunsford, *J. Phys. Chem.*, **76**, 2860 (1972).
(13) N. G. Maksimov, V. F. Anufrienko, and K. G. Ione, *Dokl. Akad. Nauk SSSR*, **212**, 142 (1973).
(14) Y.-Y. Huang and E. F. Vansant, *J. Phys. Chem.*, **77**, 663 (1973).
(15) D. R. Flentge, J. H. Lunsford, P. A. Jacobs, and J. B. Uytterhoeven, *J. Phys. Chem.*, **79**, 354 (1975).
(16) C. C. Chao and J. H. Lunsford, *J. Phys. Chem.*, **76**, 1546 (1972).
(17) R. G. Herman, *Inorg. Nucl. Chem. Lett.*, **14**, 325 (1978).
(18) B. J. Hathaway and D. E. Billing, *Coord. Chem. Rev.*, **5**, 143 (1970).
(19) K. Klier, P. J. Hutta, and R. Kellerman, *ACS Symp. Ser.*, **No. 40**, 108 (1977).
(20) R. Kellerman and K. Klier in "Surface and Defect Properties of Solids", Vol. 4, M. W. Roberts and J. M. Thomas, Ed., Billing & Sons, London, 1975, pp 1–33.
(21) P. J. Hutta, Ph.D. Dissertation, Lehigh University, Bethlehem, PA, 1974, p 40.
(22) P. E. Riley and K. Seff, *Inorg. Chem.*, **13**, 1355 (1974).
(23) P. Gallezot, Y. Ben Taarit, and B. Imelik, *J. Catal.*, **26**, 295 (1972).
(24) I. E. Maxwell and J. J. deBoer, *J. Phys. Chem.*, **79**, 1874 (1975).
(25) W. B. Williamson and J. H. Lunsford, *J. Phys. Chem.*, **80**, 2664 (1976).
(26) R. C. Slade, A. A. G. Tomlinson, B. J. Hathaway, and D. E. Billing, *J. Chem. Soc. A*, 61 (1968).
(27) R. Barbucci, A. Bencini, and D. Gatteschi, *Inorg. Chem.*, **16**, 2117 (1977).
(28) H. Elliott, B. J. Hathaway, and R. C. Slade, *J. Chem. Soc. A*, 1443 (1966).
(29) K. T. McGregor and W. E. Hatfield, *J. Chem. Soc., Dalton Trans.*, 2448 (1974).
(30) D. M. Duggan, R. G. Jungst, K. R. Mann, G. D. Stucky, and D. N. Hendrickson, *J. Am. Chem. Soc.*, **96**, 3443 (1974).
(31) B. J. Hathaway, *J. Chem. Soc., Dalton Trans.*, 1196 (1972).
(32) F. A. Cotton and G. Wilkinson, "Advanced Inorganic Chemistry", Interscience, London, 1966, p 837.

Contribution from the Chemistry Department, University of Otago, Dunedin, New Zealand

Paramagnetic Organometallic Molecules. 6.[1] Line Widths and Line Shapes in ESR Spectra of Organometallic Radicals

BARRIE M. PEAKE,* PHILIP H. RIEGER,*† BRIAN H. ROBINSON,* and JIM SIMPSON

Received September 8, 1978

The sources of line broadening and line-shape distortion in isotropic ESR spectra of organometallic radicals containing two or more equivalent nuclei have been examined in some detail. Second-order hyperfine splittings are shown to lead to asymmetric line shapes in both isotropic and frozen-solution spectra. The X-band and Q-band ESR spectra of the $C_6H_5CCo_3(CO)_9$ radical anion have been analyzed as a test of the theory. Computer simulations of the experimental isotropic spectra show that the principal line-width contribution results from incomplete averaging of anisotropies in the **g** and hyperfine tensors.

Introduction

In previous reports of the electron spin resonance (ESR) spectra of tricobalt carbon enneacarbonyl radical anions, $YCCo_3(CO)_9^-$,[2] markedly asymmetric line shapes have been noted, and a variety of explanations have been offered. In this paper, we examine in detail the factors which contribute to line shapes and line widths in the ESR spectra of organometallic radicals and radical ions. We will show that asymmetric line shapes are expected whenever the ESR spectrum has hyperfine splitting due to two or more equivalent nuclei. The theory is tested by a line-shape and line-width analysis of the ESR spectrum of the $C_6H_5CCo_3(CO)_9$ radical anion which employed computer simulation of the experimental spectra.

Theory

Isotropic ESR Spectra. Solution ESR spectra of radicals with one unpaired electron can be interpreted in terms of the spin Hamiltonian

$$H = \langle g\rangle\mu_B\vec{B}\cdot\vec{S} + \sum_i \langle A_i\rangle\vec{I}_i\cdot\vec{S} \qquad (1)$$

where $\langle g\rangle$ is the isotropic g factor, μ_B is the Bohr magneton, $\vec{B}$ is the magnetic flux density, $\langle A_i\rangle$ is the isotropic hyperfine coupling constant of the ith nucleus, and $\vec{S}$ and $\vec{I}_i$ are the electron and nuclear spin operators. If the magnetic field defines the axis of quantization (taken to be the Z axis), eq 1 can be written

$$H = \langle g\rangle\mu_B BS_Z + \sum_i \langle A_i\rangle[I_{iZ}S_Z + \tfrac{1}{2}(I_{i+}S_- + I_{i-}S_+)] \qquad (2)$$

† On leave from Brown University, Providence, R.I.

If product wave functions $|m_S, m_1, m_2, \ldots\rangle$ are used as a basis set, eq 2 can be used to predict ESR lines, to second order in perturbation theory, at field positions

$$B = B_0 - \sum_i \langle a_i\rangle m_i - \sum_i \frac{\langle a_i\rangle^2}{2B}[I_i(I_i+1) - m_i^2] \qquad (3)$$

where I_i and m_i are the nuclear spin and Z-component quantum number of the ith nucleus, $\langle a_i\rangle = \langle A_i\rangle/\langle g\rangle\mu_B$ is the hyperfine coupling constant in magnetic flux density units, and $B_0 = h\nu_0/\langle g\rangle\mu_B$ is the center field when the microwave frequency is ν_0.

If the nuclear spins are completely equivalent, that is equivalent both instantaneously and over a time average, then it is appropriate to describe the spin system in the "coupled representation" with the quantum numbers J and M of the total nuclear spin angular-momentum operators $\vec{J} = \sum\vec{I}_i$.[3,4] In the coupled representation, the spin Hamiltonian is

$$H = \langle g\rangle\mu_B BS_Z + \langle A\rangle[I_ZS_Z + \tfrac{1}{2}(J_+S_- + J_-S_+)] \qquad (4)$$

and the zero-order basis set of nuclear spin wave functions consists of linear combinations of the product wave functions which are eigenfunctions of J^2, J_Z, and the appropriate symmetry operators.

In the case of three equivalent spin $^7/_2$ nuclei, 11 values of J are found, ranging from $J = {}^1/_2$ to $J = {}^{21}/_2$. The 22 basis functions corresponding to $J = {}^{21}/_2$ are of the symmetry type A_1 and include all possible values of M ($\pm{}^{21}/_2, \pm{}^{19}/_2, \ldots, \pm{}^1/_2$). The four basis functions corresponding to $J = {}^1/_2$ are of symmetry type E and include $M = \pm{}^1/_2$. The symmetries of the other basis functions for this case are given in Table I.

0020-1669/79/1318-1000$01.00/0 © 1979 American Chemical Society

Table I. Nuclear Spin States for Three Spin $^7/_2$ Nuclei

J	symmetry	degeneracy
$^{21}/_2$	A_1	1
$^{19}/_2$	E	2
$^{17}/_2$	$A_1 + E$	3
$^{15}/_2$	$A_1 + A_2 + E$	4
$^{13}/_2$	$A_1 + 2E$	5
$^{11}/_2$	$A_1 + A_2 + 2E$	6
$^9/_2$	$2A_1 + A_2 + 2E$	7
$^7/_2$	$A_1 + A_2 + 3E$	8
$^5/_2$	$A_1 + A_2 + 2E$	6
$^3/_2$	$A_1 + A_2 + E$	4
$^1/_2$	E	2

With the appropriate basis functions, ESR lines are predicted from eq 4, to second order in perturbation theory, at field positions given by eq 5. Thus the line positions are

$$B = B_0 - \langle a\rangle M - \frac{\langle a\rangle^2}{2B}[J(J+1) - M^2] \qquad (5)$$

functions of both J and M.

To first order in perturbation theory, eq 3 and 5 give identical predictions. For three equivalent spin $^7/_2$ nuclei, 22 equally spaced lines are expected with intensity ratios 1:3:6:10:15:21:28:36:42:46:48:48:46.... To second order, the degeneracies of the lines are partially lifted, and further splitting is predicted according to both eq 3 and 5. Consider the $M = {}^{17}/_2$ "line", for example, which to first order is sixfold degenerate. Equation 5 predicts splitting into three lines of degeneracies 1, 2, and 3 at field positions given by eq 6. For

$$\begin{aligned} B(J = {}^{21}/_2) &= B_0 - ({}^{17}/_2)\langle a\rangle - 97\langle a\rangle^2/4B \\ B(J = {}^{19}/_2) &= B_0 - ({}^{17}/_2)\langle a\rangle - 55\langle a\rangle^2/4B \\ B(J = {}^{17}/_2) &= B_0 - ({}^{17}/_2)\langle a\rangle - 17\langle a\rangle^2/4B \end{aligned} \qquad (6)$$

a $YCo_3(CO)_9$ radical anion, $\langle a\rangle$ is about 3.5 mT; in the X-band spectrum $\langle a\rangle/B$ is on the order of 0.01 so that the second-order shifts are on the order of $\langle a\rangle/10$ or about 0.35 mT. Equation 3 also predicts second-order splittings but of a rather different nature. Again taking the $M = {}^{17}/_2$ line as an example, two threefold degenerate components would be expected corresponding to the nuclear spin configurations ($^7/_2$, $^7/_2$, $^3/_2$) and ($^7/_2$, $^5/_2$, $^5/_2$). The predicted field positions are

$$\begin{aligned} B({}^7/_2,{}^7/_2,{}^3/_2) &= B_0 - ({}^{17}/_2)\langle a\rangle - 41\langle a\rangle^2/4B \\ B({}^7/_2,{}^5/_2,{}^5/_2) &= B_0 - ({}^{17}/_2)\langle a\rangle - 45\langle a\rangle^2/4B \end{aligned} \qquad (7)$$

If $\langle a\rangle/B$ is on the order of 0.01, the second-order splitting is about 0.035 mT, an order of magnitude smaller than the splittings predicted by eq 5. The distinction between the two predictions is that eq 5 and 6 are appropriate if the nuclei are completely equivalent, that is, equivalent both instantaneously and on the time average. If the nuclei are equivalent on the time average, but not instantaneously (perhaps because of some fluxional behavior), then the coupled representation is not appropriate, and eq 4 and 7 apply. Thus the size and nature of second-order splittings (or line shapes attributable to such splittings) can be used as evidence for or against complete equivalence of nuclear spins. It should be noted, however, that if the nuclei are not instantaneously equivalent, but are equivalent over a time average, then the temporal process by which the coupling constants are modulated would be expected to lead to recognizable line width contributions (see below).[3]

In the case of ESR spectra of $YCo_3(CO)_9$ radical anions, the second-order splittings are, by either prediction, less than the narrowest line widths and therefore are unresolved. However, eq 6 suggests that the shape of the envelope of unresolved components should be markedly asymmetrical. Since the second-order shifts are always to low field and increase with increasing J, the envelope of lines corresponding to a given value of M is expected to have a sharp high-field cutoff and a long tail to low field. For three or more equivalent nuclei, the degeneracies of the components generally decrease with increasing J, and the asymmetry of the envelope is further enhanced. Thus an asymmetric line shape is a general expectation for ESR spectra of species containing two or more completely equivalent nuclei. The effect is more pronounced for nuclei of high spin and large isotropic coupling constant. Conversely, the effect is reduced in spectra obtained at higher microwave frequency. Thus lines in a Q-band ($\nu_0 \sim 35$ GHz) spectrum should be substantially more symmetrical than those found in a X-band ($\nu_0 \sim 9$ GHz) spectrum since the second-order shifts would be smaller by a factor of 4.

Line Widths. Line broadening in ESR spectra of organometallic radicals may be due to one or more of several different mechanisms. These mechanisms fall broadly into two classes: homogeneous broadening arising from short electron-spin transverse relaxation times, T_2, and inhomogeneous broadening which affects the observed line width or line shape without affecting T_2. In the latter category are unresolved structure, including second-order splittings, and instrumental broadening through magnetic field inhomogeneity, over-modulation, saturation, or improper tuning (resulting in an admixture of the dispersion mode). Inhomogeneously broadened lines are in general non-Lorentzian, and line width contributions are not additive.

Homogeneous line-broadening contributions are additive; that is, the width of an ESR derivative line may be computed from eq 8 where T_{2i} is the transverse relaxation time of the

$$W = \frac{2\hbar}{3^{1/2}\langle g\rangle\mu_B}\sum_i T_{2i}^{-1} \qquad (8)$$

ith line-broadening mechanism. It is frequently found that line widths may be expressed as a power-series function of the quantum number M:

$$W = \alpha + \beta M + \gamma M^2 + \delta M^3 + \epsilon M^4 \qquad (9)$$

There are several mechanisms which contribute to the coefficients of eq 9, but the most common, and frequently the largest single line-broadening mechanism, is incomplete averaging of anisotropies in the **g** and hyperfine tensors by slow tumbling of the radical in solution. As the radical rotates, line positions are modulated and line-width contributions result which are proportional to τ_R, the rotational correlation time. Contributions to α, β, γ, and δ of eq 9 have been computed by Wilson and Kivelson;[5] for axially symmetric **g**- and hyperfine tensors, these are given by eq 10a–d where C =

$$\alpha/C\tau_R = (B_0\Delta\gamma)^2(4 + 3u) + \tfrac{1}{2}(b\gamma_e)^2(3 + 7u - 5uf\langle a\rangle/B_0)J(J+1) - (B_0\Delta\gamma)(\gamma_e b)(\langle a\rangle/B_0)J(J+1) \qquad (10a)$$

$$\beta/C\tau_R = 2(B_0\Delta\gamma)(b\gamma_e)(4 + 3u) - 2(B_0\Delta\gamma)^2(\langle a\rangle/B_0)(4 + 3u + 3uf) - (b\gamma_e)^2(\langle a\rangle/B_0)[(1 + u + 7uf)J(J+1) + (\tfrac{3}{2} + u)] \qquad (10b)$$

$$\gamma/C\tau_R = \tfrac{1}{2}(b\gamma_e)^2(5 - u + 5uf\langle a\rangle/B_0) - (B_0\Delta\gamma)(b\gamma_e)(\langle a\rangle/B_0)(7 + 5u + 12uf) \qquad (10c)$$

$$\delta/C\tau_R = (b\gamma_e)^2(\langle a\rangle/B_0)(1 + u + uf) \qquad (10d)$$

$2\hbar/45(3^{1/2})\langle g\rangle\mu_B$, $\gamma_e = \langle g\rangle\mu_B/\hbar$, $\Delta\gamma = (g_\parallel - g_\perp)\mu_B/\hbar$, $b = a_\parallel - a_\perp$, $u = (1 + \omega_0^2\tau_R^2)$, and $f = \omega_0^2\tau_R^2 u$. Notice that since α and β are functions of J, components of different J, but the same value of M, are expected to have different widths. Furthermore, since most terms are functions of the center field B_0, the coefficients α, β, γ, and δ are functions of the microwave frequency and are different, for example, in X-band and Q-band spectra.

The effect of the nuclear quadrupole interaction averages to zero in isotropic spectra. However, just as anisotropies in the **g** and hyperfine tensors contribute to line widths when the radical tumbles slowly in solution, line-width contributions proportional to τ_R are expected from quadrupolar coupling. For a radical with a single nucleus, or several inequivalent nuclei, line-width contributions proportional to even powers of M (α, γ, and ϵ) have been computed theoretically.[6] When two or more completely equivalent nuclei are present, the theory becomes much more complex, and the details have not been worked out. It is likely, however, that contributions to α, γ, and ϵ would still result.

Coupling of the electron-spin magnetic moment to the rotational motion of the radical in solution provides a relaxation mechanism which broadens all lines equally. The contribution to α is given approximately by[7] eq 11 where g_e is the free

$$\alpha'\tau_R/C = 5[(g_{\parallel} - g_e)^2 + 2(g_{\perp} - g_e)^2] \quad (11)$$

electron g value. The rotational correlation time is given approximately by eq 12 where V is the hydrodynamic volume

$$\tau_R = V\eta/kT \quad (12)$$

of the radical and η is the solution viscosity. Thus spin-rotational line-width contributions are expected to increase with T/η whereas the contributions arising from motional averaging of anisotropies increase with η/T.

Spin exchange between radicals or between a radical and another paramagnetic species (such as molecular oxygen) limits the lifetime of a spin state and therefore contributes to ESR line widths. Similarly electron exchange between a radical ion and the neutral parent molecules provides a line-broadening mechanism. The contributions of these mechanisms are nearly independent of M and may be expressed by[8] eq 13 where k_2 is the second-order rate constant

$$\alpha'' = (2/(3^{1/2})\gamma_e)k_2[X] \quad (13)$$

for the process and [X] is the concentration of radical in the case of spin exchange or neutral parent in the case of electron exchange. Spin exchange is often diffusion controlled for neutral radicals but is usually slower for radical ions. Even so, if k_2 is 10^9 dm^3 mol^{-1} s^{-1} and [X] is 10^{-2} mol dm^{-3}, α'' is only 0.066 mT, barely significant in most spectra of organometallic radicals. Electron exchange is usually slower than spin exchange, and thus these mechanisms would be expected to be significant only under conditions of high concentration and temperature and when other line-broadening contributions are small.

Other kinetic processes may effect line widths if they modulate either $\langle g \rangle$ or $\langle a \rangle$.[3,6] Thus a ligand-exchange or conformational equilibrium could affect line widths if the rate is in the appropriate range. Modulation of $\langle g \rangle$ broadens all lines equally and thus contributes to α. Modulation of $\langle a \rangle$ gives a contribution to γ if only one nucleus is involved, or, if two or more completely equivalent nuclei are present, the modulation of the hyperfine couplings is in-phase. If the hyperfine couplings are modulated out-of-phase, the nuclei are instantaneously inequivalent, and the line-width contributions for a given line are proportional to the square of quantum number differences; e.g., for two nuclei, the contribution is proportional to $(m_1 - m_2)^2$. If both $\langle g \rangle$ and $\langle a \rangle$ are modulated, cross terms arise which contribute to β.

A number of other line-broadening mechanisms have been suggested[9] but are probably not significant in the ESR spectra of organometallic radicals.

Frozen-Solution ESR Spectra. Spectra of frozen solutions of organometallic radicals are often useful. Time-dependent phenomena (fluxional behavior, intramolecular electron exchange, etc.) that may perturb the spectra of liquid solutions are often frozen out. Radicals generated at low temperature may be difficult to detect in liquid solution because of low spectrometer sensitivity. Dielectric loss in the solvent increases with decreasing temperature but is markedly reduced when the solution is frozen. Thus spectrometer sensitivity is usually much higher for frozen solutions than for the same sample just above the freezing point.

Frozen-solution spectra are in general much more complex than isotropic spectra, but, in favorable cases, one or more of the components of the **g** and hyperfine tensors may be evaluated by simple analysis of the frozen-solution spectrum.[10] Features are expected in the frozen-solution spectrum corresponding to orientation of each of the principal axes of the tensors in the direction of the magnetic field, and, if the hyperfine tensor is sufficiently anisotropic, the features will be resolved, and the spectrum can be interpreted.

On the assumption of axial symmetry and that the principal axes of the **g** and hyperfine tensors are coincident, the spin Hamiltonian for an oriented sample may be written as in eq 14[11] where θ is the angle between the magnetic field (the Z axis) and the principal axis of the **g** tensor; g and A are given by eq 15 and 16. When the field is parallel to the principal

$$H = g\mu_B BS_Z + AS_ZI_Z + (A_{\parallel}A_{\perp}/A)S_XI_X + A_{\perp}S_YI_Y + (g_{\parallel}g_{\perp}/g^2)[(A_{\perp}^2 - A_{\parallel}^2)/2A](\sin 2\theta)S_XI_Z \quad (14)$$

$$g = (g_{\parallel}^2 \cos^2\theta + g_{\perp}^2 \sin^2\theta)^{1/2} \quad (15)$$

$$A = (g_{\parallel}^2A_{\parallel}^2 \cos^2\theta + g_{\perp}^2A_{\perp}^2 \sin^2\theta)^{1/2}/g \quad (16)$$

axis ($\theta = 0$), lines are predicted, to second order, at field positions

$$B_{\parallel} = B_{\parallel,0} - a_{\parallel}M - (a_{\perp}^2/2B_{\parallel})[J(J+1) - M^2] \quad (17)$$

and, in the perpendicular orientation, lines are expected at

$$B_{\perp} = B_{\perp,0} - a_{\perp}M - \frac{(a_{\parallel}^2 + a_{\perp}^2)}{4B_{\perp}}[J(J+1) - M^2] \quad (18)$$

where $B_{i,0} = h\nu_0/g_i\mu_B$ and $a_i = A_i/g_i\mu_B$.

In the case of a $YCo_3(CO)_9$ radical anion, the **g** tensor is nearly isotropic, but the hyperfine tensor is quite anisotropic with $a_{\parallel} \simeq -8$ mT and $a_{\perp} \simeq 1.5$ mT. Thus in the X-band spectrum, the second-order shifts of the parallel features corresponding to $M = {}^{17}/_2$ are −0.17, −0.14, and −0.03 mT for $J = {}^{21}/_2$, ${}^{19}/_2$, and ${}^{17}/_2$, respectively. Since the observed lines are typically 2–3 mT wide, these shifts are quite negligible and do not contribute significantly to the width or shape of the lines. The perpendicular features, on the other hand, are expected to exhibit much larger shifts. Again for $M = {}^{17}/_2$, shifts are expected of −2.47, −1.40, and −0.43 mT, and it is clear that line widths and shapes would be affected.

Since ^{59}Co (and other nuclei with $I > {}^1/_2$) has a quadrupole moment, one might expect quadrupolar effects to be evident in ESR spectra of organometallic radicals containing such nuclei. Quadrupole coupling effects depend upon the electric field gradient at the nucleus and vanish when the nuclear environment is spherically symmetric. Because the trace of the quadrupole coupling tensor is zero, line positions in an isotropic spectrum are independent of quadrupole coupling. Frozen-solution or dilute single-crystal spectra, on the other hand, should show quadrupolar effects.

On the assumption of axial symmetry and coincident principal tensor axes, the quadrupolar terms in the spin Hamiltonian can be written as in eq 19[11] where P is the quadrupole coupling constant. Only the first term of eq 19 is of significance for the parallel features of the spectrum ($\theta = 0°$). It contributes only diagonal elements to the Hamiltonian matrix when a single nucleus (or several inequivalent

$$H_q = \tfrac{1}{2}P\left[\frac{3A_\parallel^2 g_\parallel^2}{g^2A^2}\cos^2\theta - 1\right]\sum_i[I_{Zi}^2 - \tfrac{1}{3}I_i(I_i+1)] - \tfrac{1}{2}P\left[\frac{g_\parallel g_\perp A_\parallel A_\perp}{g^2A^2}\sin 2\theta\right]\sum_i[I_{Zi}I_{Xi} + I_{Xi}I_{Zi}] + \tfrac{1}{4}P\left[\frac{g_\perp^2 A_\perp^2}{g^2A^2}\sin^2\theta\right]\sum_i[I_{Xi}^2 - I_{Yi}^2] \quad (19)$$

nuclei) is present. Since both the $m_S = +^1/_2$ and $m_S = -^1/_2$ states are raised in energy by the same amount, there can be no effect on the ESR spectrum. When two or more equivalent nuclei are present, the first term of eq 19 leads to off-diagonal matrix elements connecting nuclear spin states of like symmetry and M quantum number but different J values. Thus, for example, in the case of three equivalent spin $^7/_2$ nuclei, there are six nuclear spin states with $M = ^{17}/_2$. The two states of A_1 symmetry, $J = ^{21}/_2$ and $J = ^{17}/_2$, are mixed as are the four states of E symmetry, $J = ^{19}/_2$ and $J = ^{17}/_2$. For small P ($\ll A_\perp$), the selection rules, $\Delta m_S = \pm 1$, $\Delta J = 0$, $\Delta M = 0$, are still valid, and predicted line positions are unaffected. For larger values of P ($\sim A_\perp$), the $\Delta J = 0$ selection rule breaks down, and "forbidden" transitions emerge at both higher and lower field which should be well resolved from the "allowed" transitions which remain virtually unshifted at their positions for $P = 0$.

In the perpendicular orientation ($\theta = 90°$), the third term of eq 19 mixes nuclear spin states of a given M with states of the same symmetry, and $M' = M + 1$. Here, both the $\Delta J = 0$ and $\Delta M = 0$ selection rules fail, and both shifts of "allowed" transitions and the emergence of "forbidden" transitions are expected. The situation is extremely complicated and has not been analyzed in detail.

Results and Discussion

Isotropic ESR Spectra. The X-band ESR spectrum of the $C_6H_5CCo_3(CO)_9$ radical anion in THF solution consists of 22 hyperfine lines as expected for a radical with three equivalent spin $^7/_2$ nuclei. Spectra obtained at +40 °C and −20 °C are shown in Figures 1a and 2a. The most notable features of the spectra are the markedly asymmetric line shapes, particularly of the central lines, and the much greater width of the outer lines. The widths of lines with larger values of M are strongly temperature dependent whereas the central lines vary in width hardly at all over the temperature range −60 to +60 °C. The outermost lines, $M = \pm^{21}/_2$, are generally observable only at or above room temperature, and as the temperature is lowered, further lines broaden beyond detection.

Because of the markedly asymmetric line shapes, it is difficult to measure line positions accurately. At 60 °C the nondegenerate $\pm^{21}/_2$ lines were well resolved and could be used to determine the isotropic parameters $\langle g\rangle$ and $\langle a\rangle$. When the $\pm^{21}/_2$ lines were not observable or too broad to measure accurately, the $\pm^{19}/_2$ and $\pm^{17}/_2$ lines were used with second-order shifts computed by taking appropriate weighted averages over the $J = ^{21}/_2$, $^{19}/_2$, and $^{17}/_2$ components. The measured values of $\langle g\rangle$ and $\langle a\rangle$ are, respectively, 2.013 ± 0.001 and −3.58 ± 0.01 mT.[12]

The ESR spectrum of the $C_6H_5CCo_3(CO)_9$ anion, obtained with a Q-band spectrometer ($\nu_0 = 34.66$ GHz), is shown in Figure 3a. As expected from the theory of second-order shifts, the line shapes are much less asymmetric than in the X-band spectra. Sixteen of the 22 lines are clearly visible, and these are assigned with the help of simulation techniques (see below) to the lines with M ranging from $-^{17}/_2$ to $+^{13}/_2$. Thus the line with maximum derivative amplitude corresponds to $M = -^5/_2$.

Frozen-Solution ESR Spectra. The ESR spectrum of a frozen THF solution of the $C_6H_5CCo_3(CO)_9$ radical anion,

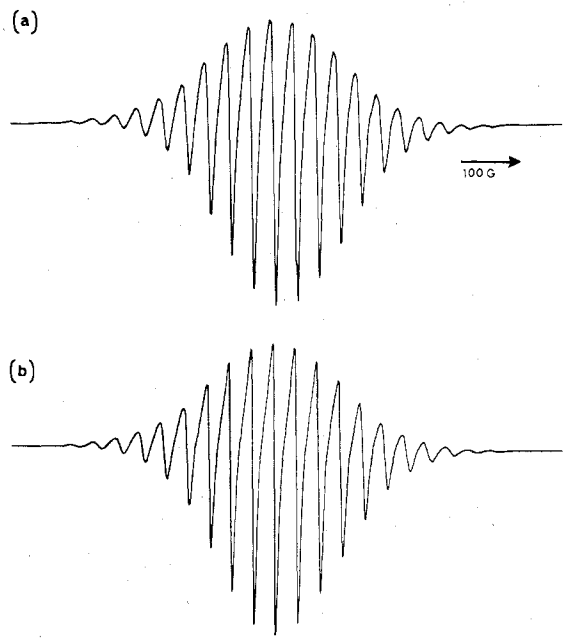

Figure 1. X-band ESR spectrum of $C_6H_5CCo_3(CO)_9$ radical anion: (a) experimental spectrum of radical in THF solution at 40 °C; (b) computer-simulated spectrum.

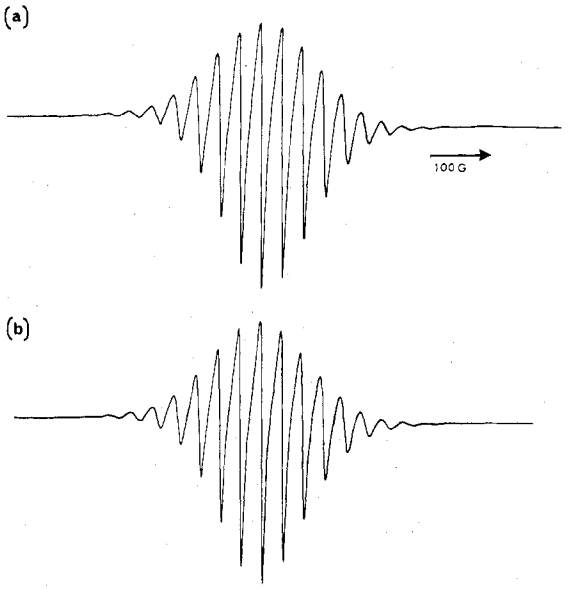

Figure 2. X-band ESR spectrum of $C_6H_5CCo_3(CO)_9$ radical anion: (a) experimental spectrum of radical in THF solution at −20 °C; (b) computer-simulated spectrum.

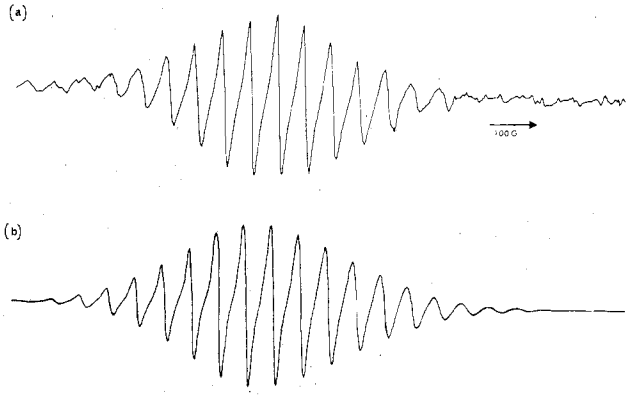

Figure 3. Q-band ESR spectrum of $C_6H_5CCo_3(CO)_9$ radical anion: (a) experimental spectrum of radical in THF solution at room temperature; (b) computer-simulated spectrum.

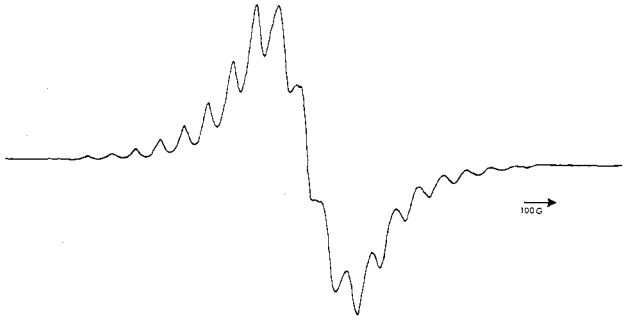

Figure 4. X-band ESR spectrum of frozen THF solution of $C_6H_5CCo_3(CO)_9$ radical anion.

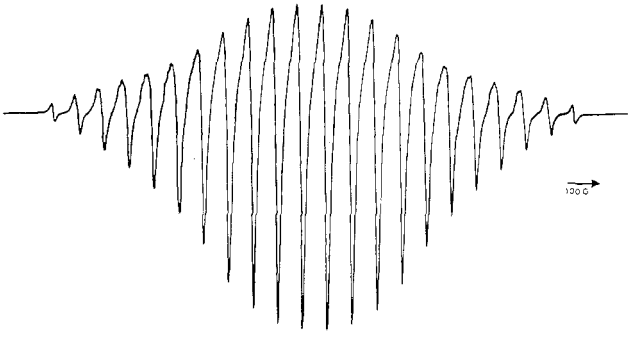

Figure 5. Computer-simulated spectrum of the $C_6H_5CCo_3(CO)_9$ radical anion with constant component widths of 0.5 mT.

obtained at −140 °C, is shown in Figure 4. Most of the 22 expected parallel features are well resolved and are easily identified. Second-order corrections to the parallel spectrum, eq 17, are small so that these features are easily interpretable by use of first-order theory: $g_{\parallel} = 1.996 \pm 0.002$, $a_{\parallel} = -7.90 \pm 0.001$ mT.[12] The perpendicular features, on the other hand, are completely unresolved. The lack of resolution is due to two factors: (1) $a_{\perp}$ is −1.42 mT, less than the line widths of 2–3 mT; (2) second-order shifts, given by eq 18, are large, often larger than $a_{\perp}$, so that many more than 22 lines are expected.

No "forbidden" transitions are observed in the parallel regions of the spectrum. Similarly, no extra lines were observed in the dilute single-crystal spectrum of $SCo_3(CO)_9$, reported by Strouse and Dahl,[13] which was much better resolved than the frozen-solution spectrum reported here. Thus we can conclude that the quadrupolar coupling, while not necessarily zero, is certainly small with $P \ll g_{\perp}\mu_B a_{\perp}$.

A series of tricobalt carbon cluster molecules has recently been studied by nuclear quadrupole resonance spectroscopy.[14] For the phenyl derivative, $P = 2.66$ MHz, and although the principal axes of the quadrupolar coupling are quite different from those of the hyperfine tensor and the quadrupolar coupling constant is probably slightly different in the radical anion, P is indeed much smaller than $|g_{\perp}\mu_B a_{\perp}|$ which, for $C_6H_5CCo_3(CO)_9^-$, is about 40 MHz.

Spectrum Simulations. In order to verify the explanation of the line shapes observed in the ESR spectra of $YCCo_3(CO)_9$ radical anions, spectra were computer simulated with line positions calculated with eq 5. A simulated spectrum, computed assuming a constant component line width of 0.5 mT, is shown in Figure 5. From a comparison of Figures 1a and 2a, it is seen that the line shapes, particularly in the center of the spectrum, are qualitatively reproduced. However, the outer lines are much more prominent in the simulated spectrum, suggesting line-width contributions proportional to M^2. Since the parameters of eq 10 are known, the line-width contributions from modulation of the **g**- and hyperfine-tensor anisotropies can be computed given a value of τ_R, the rotational correlation time. For example, if τ_R is assumed to be 10^{-11} s, a reasonable expectation for solutions near room temperature, the contribution to the $J = {}^{21}/_{2}$, $M = +{}^{21}/_{2}$ line is 1.6 mT, but the contribution to the $J = {}^{1}/_{2}$, $M = +{}^{1}/_{2}$ line is only 0.02 mT. Clearly, if the components were that sharp, second-order splittings would be resolved near the center of the spectrum; thus there must be other contributions to the line widths.

Table II. Line-Width Parameters Used in Spectrum Simulations

T/K	τ_R/(10^{-11} s)[a]	α'/mT[b]	T/K	τ_R/(10^{-11} s)[a]	α'/mT[b]
233	6.5	0.50	293	1.7	0.40
253	4.5	0.45	313	1.5	0.45
273	2.75	0.45	333	1.0	0.55

[a] ±15%. [b] ±0.05 mT.

In testing the hypothesis that eq 10a–d account for the variation in line width among components, an additional contribution, α', was added to all component widths and the two parameters τ_R and α' were adjusted to give the best fit to the experimental spectra. Simulations were undertaken for X-band spectra of the $Y = C_6H_5$ radical anion at temperatures ranging from −40 to +60 °C and for the room-temperature Q-band spectrum. The simulations of the X-band spectra which used the values of τ_R and α' given in Table II are compared with experimental spectra in Figures 1b and 2b. The simulation of the Q-band spectrum ($\tau_R = 2.5 \times 10^{-11}$ s, $\alpha' = 0.8$ mT) is given in Figure 3b.

The match of experimental and simulated spectra is quite good overall. A small discrepancy, most noticeable at lower temperatures, is an overestimate of the line width term, β, eq 10b, which causes the lines in the simulated spectra to be too broad at the high-field end of the spectrum and too sharp at the low-field end. If the experimental value of $\Delta\gamma$ were too large, then β would be overestimated. The Q-band widths are much more strongly dependent on $\Delta\gamma$, however, and can be simulated satisfactorily with the same set of parameters used to simulate the X-band spectra. It is thus more likely that the discrepancy arises from another contribution to γ which is not included in the simulations. To compensate for the missing contribution to γ, τ_R, and thus β, would be overestimated. The missing contribution may be due to the quadrupolar interaction. However, since the theory of quadrupolar line-width contribution has not been developed for radicals with equivalent nuclei, there seems little more we can do.[15] The effect is small, and, even with an adequate theory, it would be difficult to prove conclusively that it is quadrupolar in origin.

The small increase in α' at the higher temperatures may be due to a spin–rotation contribution to the line widths. With the values of $g_{\parallel}$ and $g_{\perp}$ for $C_6H_5CCo_3(CO)_9^-$, together with τ_R from Table II, eq 11 suggests negligible spin–rotation contributions below about 293 K and a contribution of about 0.06 mT at 333 K, consistent, within the uncertainties of the theory and data, with the results shown in Table II.

By far the largest part of α' remains unexplained. The residual line width is only weakly temperature dependent but appears to increase with microwave frequency. Quadrupolar contributions might account for some of the residual width, but these would be expected to be proportional to τ_R and independent of microwave frequency. Of the line-broadening mechanisms known, only motional averaging of the **g**-tensor anisotropy and modulation of the isotropic g value should give field-dependent line-width contributions. The former contribution has already been explicitly accounted for in the simulations, and the latter seems unlikely on several grounds.

Experimental Section

Phenyl tricobalt carbon enneacarbonyl was synthesized by the literature method and reduced to the radical anion by sodium in THF

solution. X-band ESR spectra were obtained with a Varian E-4 spectrometer equipped with a variable-temperature accessory. Temperatures quoted in this paper were read from the uncalibrated temperature controller and are thus of qualitative significance only. The microwave frequency was measured with a Systron Donner 6054A frequency counter. The magnetic-field calibration of the E-4 spectrometer was checked with a proton resonance gaussmeter. Q-band ESR spectra were obtained by Dr. Ira Goldberg, Rockwell Science Center, Thousands Oaks, CA, with a Varian TE_{011} cavity, Varian V-4561 Q-band microwave bridge, a modified Varian V-4502 spectrometer, and a Magnion 15-in. magnet.

Acknowledgment. Acknowledgment is made to the donors of the Petroleum Research Fund, administered by the American Chemical Society, for partial support of this research. We also thank the Research Committee of the New Zealand Universities Grants Committee for financial support.

Registry No. $C_6H_5CCo_3(CO)_9^-$, 61024-80-4.

References and Notes

(1) Part 5: P. Dawson, B. M. Peake, P. H. Rieger, B. H. Robinson, and J. Simpson, submitted for publication in *Inorg. Chem.*
(2) T. W. Matheson, B. M. Peake, B. H. Robinson, J. Simpson, and D. J. Watson, *J. Chem. Soc., Chem. Commun.*, 894 (1973); B. M. Peake, B. H. Robinson, J. Simpson, and D. J. Watson, *Inorg. Chem.*, **16**, 405 (1977).
(3) G. K. Fraenkel, *J. Phys. Chem.*, **71**, 139 (1967).
(4) R. W. Fessenden, *J. Chem. Phys.*, **37**, 747 (1962).
(5) R. Wilson and D. Kivelson, *J. Chem. Phys.*, **44**, 154 (1966).
(6) J. H. Freed and G. K. Fraenkel, *J. Chem. Phys.*, **39**, 326 (1963).
(7) P. W. Atkins and D. Kivelson, *J. Chem. Phys.*, **44**, 169 (1966).
(8) J. E. Wertz and J. R. Bolton, "Electron Spin Resonance", McGraw-Hill, New York, 1972, p 201.
(9) W. B. Lewis and L. O. Morgan, *Transition Met. Chem.*, **4**, 33 (1968).
(10) Reference 8, p 154.
(11) N. M. Atherton, "Electron Spin Resonance", Ellis Harwood, Chichester, England, 1973, p 222.
(12) The negative signs assumed for $\langle a \rangle$, $a_{\parallel}$, and $a_{\perp}$ are based on theory and analogy with similar radicals. See ref 13.
(13) C. E. Strouse and L. F. Dahl, *Discuss. Faraday Soc.*, **47**, 93 (1969).
(14) D. C. Miller and T. B. Brill, *Inorg. Chem.*, **17**, 240 (1978).
(15) Using the experimental quadrupole coupling constant, $P = 2.66$ MHz,[14] and the theoretical quadrupolar line-width contribution for radicals with a single nucleus (ref 11, p 350), one can estimate a line-width contribution on the order of 0.0003 mT when $\tau_R = 6 \times 10^{-11}$ s. Although this is quite negligible, the contribution might be significantly larger when three equivalent nuclei are taken into account.

Contribution from the Radiation Laboratory, University of Notre Dame, Notre Dame, Indiana 46556

Photochemical Pathways of the Dimeric, Mixed Dimer, and Monomeric Sulfophthalocyanines of Cobalt(III) and Iron(II)

G. FERRAUDI

Received July 27, 1978

The photochemical reactivity of the dimeric, mixed dimer, and monomeric sulfophthalocyanines of cobalt(III) and iron(II) was investigated by steady-state and flash irradiations. The dimeric species photodissociated into sulfophthalocyanine radicals which were coordinated to either Co(III) or Fe(II) metal centers. Reactions of such intermediates were investigated by interception with alcohols and O_2. Also, photoredox reactions were detected with monomeric acidocobalt(III) sulfophthalocyanines. These processes produce the oxidation of the acido ligands (Cl^-, Br^-, N_3^-, I^-) and the reduction of the metal center. The photoredox dissociation was also investigated by using mixed dimers of the cobalt sulfophthalocyanines with $Cr(bpy)_3^{3+}$ and $Ru(bpy)_3^{2+}$. The photogeneration of sulfophthalocyanine radicals was observed as a general reaction which was produced by excitation of either the $Cr(bpy)_3^{3+}$ or $Ru(bpy)_3^{2+}$ units in the mixed dimer. The nature of the reactive excited states involved in the various photochemical reactions of the sulfophthalocyanines of Co(II), Co(III), Cu(II), and Fe(II) is discussed.

Introduction

The photochemistry of the dimeric and monomeric sulfophthalocyanines of copper(II) and cobalt(II) have been recently investigated.[1,2] Such a study has demonstrated that dimeric species are photodissociated by irradiation of the ultraviolet bands. Copper(II)–ligand radicals and sulfophthalocyanines with cobalt(I) and cobalt(III) metal centers are the primary products of these reactions. In addition, photoredox processes of the monomeric cobalt(II) and copper(II) sulfophthalocyanines were observed when these species were irradiated in the presence of hydrogen donors. These photochemical properties of the dimeric and monomeric complexes were related to the population of a ligand-centered excited state which is probably an $n\pi^*$ state of the ligand. In this regard, it seems that there is some parallelism between the photochemistries of the sulfophthalocyanines and porphyrins.[3,4] In fact, it has been reported that population of $n\pi^*$ excited states of the porphyrins induces their reduction by tertiary amines.

Also, a photoredox process has been briefly reported for a methylcobalt(III) sulfophthalocyanine by Day et al.[5] This reaction can probably be described as the same homolytic photodissociation of the metal–carbon bond which is observed with other methylcobalt(III) macrocyclic complexes.[6-8] Nevertheless, the behavior of the methylcobalt(III) sulfophthalocyanine contrasts with the photochemistries of the sulfophthalocyanines of copper(II) and cobalt(II). These differences suggest that a low-energy charge-transfer ligand-to-metal, CTTM, excited state is the photoactive state of the methyl complex.[9] In this regard, one may expect that the photochemistry of some sulfophthalocyanines should have the combined features of the reactions which are originated in either charge-transfer or ligand-centered states.[9] In such a case, the nature of the ligands attached to the metal center in axial positions will have a large influence on the nature of the photochemical process.

The study of the photochemistry of the sulfophthalocyanines of the transition-metal ions has been continued in this work by use of complexes with d^6 metal centers, Fe(II) and Co(III).[2] The results, obtained with monomeric and dimeric species, are compared with those of the copper(II) and cobalt(II) complexes.

Experimental Section

Photochemical Procedures. Steady-state irradiations were carried out with an experimental setup that was previously described in some detail.[1] A 300-W xenon Varian lamp, combined with collimating filters, lenses, and a high intensity Bausch and Lomb monochromator, was used for ultraviolet–visible photolyses. The entrance and exit

0020-1669/79/1318-1005$01.00/0 © 1979 American Chemical Society